Numerical Study of Screening Current on HTS Stellarator Coil and Experimental Validation Through Screening Current Induced Voltage

Geonyoung Kim, Nicolo Riva, Sehyun Cho, Dongwoo Lee, Wonseok Jang, Hyunsoo Park, Chaemin Im, Jung Tae Lee, Yufan Yan, Jaemin Kim, Jeseok Bang, Wei Guo, Nicolò Foppiani, Seungyong Hahn, and Sangjin Lee

***Abstract*—This study presents a numerical model for simulating screening current distribution in REBCO stellarator coils using a distributed-circuit approach with widthwise segmentation. By applying an equipotential assumption along the conductor‘s width, which can generally be applied, the model reduces the number of circuit elements, enabling efficient calculation of electromagnetic and thermal parameters such as current distribution and AC loss within a short time. Experimental validation using a 1/20-scale stellarator coil confirmed the model’s accuracy in predicting the effects of screening current on voltage profiles during repeated operations. The results indicate that voltage measurements can effectively estimate screening currents in high-temperature superconducting (HTS) magnets.**

***Index Terms*—Distributed-circuit, fusion, screening current, screening current induced voltage, stellarator.**

I. Introduction

In the past decade, with the advancements in high-temperature superconducting (HTS) magnet technology [1], [2], [3], [4], [5], [6], there has been growing anticipation that fusion magnets could also adopt HTS technology [7], [8], [9], [10], [11]. Many startups are actively developing HTS magnets [12], [13], [14], [15], showing significant results. No-insulation (NI) technique [16], which played a significant role in achieving the world‘s highest DC magnetic field [17], has greatly contributed to these achievements. However, challenges such as field distortion [18], [19] and stress caused by screening currents [20], [21], [22] remain unresolved. Moreover, studies that address the aforementioned issues under the assumption of using HTS in stellarators are rare and have only recently begun to gain attention. To analyze these screening currents, the finite element method (FEM) has been widely used [23], [24], [25], and many studies have demonstrated its consistency with experimental results [26], [27]. Nevertheless, for complex shapes like stellarator coils, the time and computational power required for FEM increase significantly, highlighting the need for more efficient analysis methods.

In this study, we developed a numerical model to simulate the screening current distribution in REBCO stellarator coils using a distributed-circuit method with widthwise segmentation [28], [29], [30]. The model was applied to analyze current distribution and AC loss in a full-scale stellarator module coil designed by Proxima Fusion, comparing the results across three different operating current scenarios. Experimental validation with a 1/20-scale stellarator coil confirmed the model’s accuracy, particularly in predicting the impact on voltage (or screening current induced voltage) during operations.

II. Method: Distributed-Circuit Model With Widthwise Segmentation

We adopted a distributed-circuit model based on the partial element equivalent circuit (PEEC) method [31], [32], [33], [34] to simulate the screening current distribution (or nonuniform current distribution) within the conductor. Although more accurate results can be obtained when the NI coil is expressed with all the circuit components, the computation time should be considered. To reduce the circuit component, we set the widthwise equipotential assumption, which means that the electrical potential along the width of the REBCO conductor is the same as shown in Fig. 1. redThis assumption is generally valid for magnet simulations, as the current flowing in the width direction of the superconducting tape is relatively negligible and has

Received 25 September 2024; revised 31 December 2024; accepted 23 January 2025. Date of publication 29 January 2025; date of current version 10 March 2025. This work was supported in part by the National R&D Program through the National Research Foundation of Korea (NRF) funded by Ministry of Science and ICT under Grant 2022M3I9A1073924 and in part by the Applied Superconductivity Center, Electric Power Research Institute of Seoul National University. *(Corresponding author: Sangjin Lee.)*

Geonyoung Kim, Sehyun Cho, Dongwoo Lee, Wonseok Jang, Hyunsoo Park, Jung Tae Lee, Seungyong Hahn, and Sangjin Lee are with the Department of Electrical and Computer Engineering, Seoul National University, Seoul 08826, South Korea (e-mail: sjlee03@snu.ac.kr).

Nicolo Riva, Wei Guo, and Nicolò Foppiani are with Proxima Fusion, 81369 München, Germany.

Chaemin Im is with Applied Superconductivity Center, Electric Power Research Institute, Seoul National University, Seoul 08826, South Korea.

Yufan Yan was with Applied Superconductivity Center, Electric Power Research Institute, Seoul National University, Seoul 08826, South Korea. She is now with Lawrence Berkeley National Laboratory, Berkeley, CA 94720 USA.

Jaemin Kim was with Applied Superconductivity Center, Electric Power Research Institute, Seoul National University, Seoul 08826, South Korea. He is now with Standard Magnet Inc., Seoul 05840, South Korea.

Jeseok Bang is with National High Magnetic Field Laboratory, Florida State University, Tallahassee, FL 32306 USA.

Color versions of one or more figures in this article are available at https://doi.org/10.1109/TASC.2025.3535859.

Digital Object Identifier 10.1109/TASC.2025.3535859

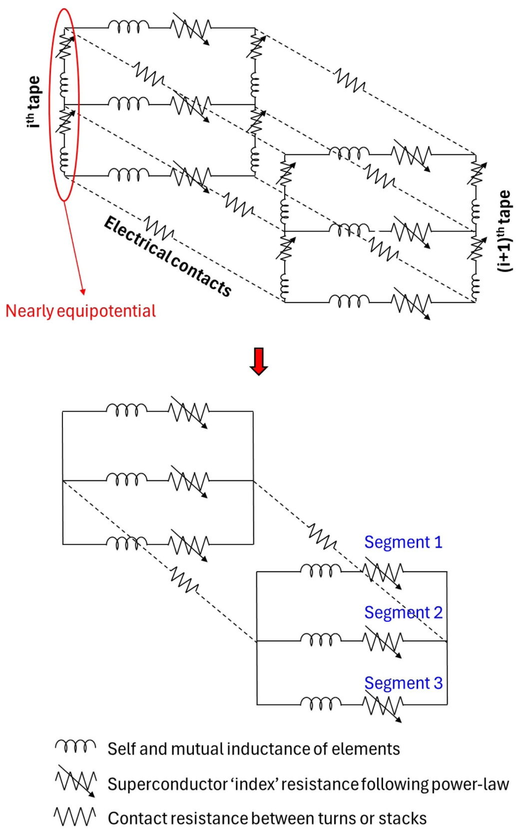

Fig. 1. Schematic drawing of the small block of distributed-circuit model based on the PEEC. Each tape is divided in widthwise direction to simulate screening current distribution, and each divided pieces are named 'segment'. With equipotential assumption, which can be considered in general, the nodes within the red circle is merged for simplification of model. The conductor is expressed by combination of self-inductances, mutual inductances, and the 'index' resistance following the power-law V-I characteristics. The electrical contact between conductor is expressed by turn-to-turn contact resistances.

little impact on the analysis results of the current distribution in the tape's length direction. Therefore, each lengthwise element of the conventional PEEC model for a NI coil is substituted by widthwise segmented element while the electrical contact between adjacent tapes is characterized by a single path with a resistance.

For the simulation, the mutual inductances between circuit elements are required. We used the numerical integration method with the well-known Neumann formula [35] for two line segments. The closed-form solution of mutual inductance between two line segments is determined according to the positional relationship between them. Then, the mutual inductance between two thin conductors can be numerically integrated by the sum of the inductance of the pairs of two line segments within the conductors.

Contact resistance R_c between adjacent tapes were calculated by following equation:

$$R_c = \frac{\rho_{ct}}{S}, \quad (1)$$

where ρ_{ct} and S represent the contact resistivity between conductors [36], [37], [38], [39] and the contacted area, respectively. Moreover, superconducting 'index' resistance was calculated with consideration of field-dependent properties of REBCO conductor. We adopted the practical fitting function suggested by D. K. Hilton et al. [40]. Then, a system of nonlinear first-order differential equations was formulated according to the simulation cases, and it was solved by the MATLAB's built-in solver.

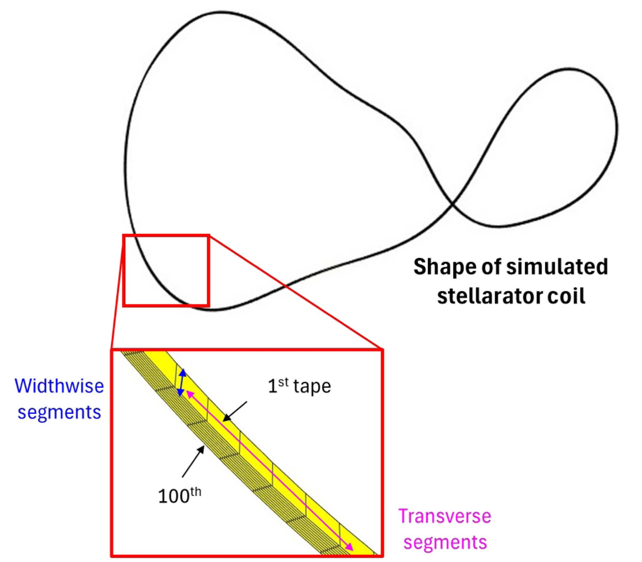

Fig. 2. Schematic of real-scale stellarator module coil. The cable is assumed to consist of 100 tapes of REBCO conductor.

III. Case Study: Simulation of 100-Tape REBCO Stellarator Module Coil in Real Scale

Simulation target for this study was a real-scale stellarator coil designed by Proxima Fusion. Approximately 4-m wide module coil was designed with consideration of target magnetic field distribution and bending strain. We assumed the module coil is made by one turn of stacked cable with 12-mm square cross-section. As shown in Fig. 2, the cable consisted of 100 tapes of REBCO conductor. We assumed that the Faraday Factory Japan's conductor is used for the cable, and the operating temperature is 4.2 K. These assumptions are for convenience of simulation, so they might not be applied for the real magnet.

For the simulation of widthwise distribution of screening current, each tape was subdivided into 16 segments. The operating currents were assumed to 20 kA, 50 kA, and 100 kA while the coil charging times were assumed to be identically one hour. Then, the operating current was assumed to be maintained for another single hour. Furthermore, we calculated the inductance between each element, and the results are shown in Fig. 3. To calculate this inductance matrix, total of 1.6 hours was required by our numerical integration method.

By the aforementioned assumptions and inductance matrix, we simulated the current distribution and AC loss. These parameters are crucial to estimate the electromagnetic and thermal properties of the coil. The screening current distribution for each operating current case were simulated as shown in Fig. 4. The results are the current distribution in the cross-section of the coil at right after the charging (1 h). Due to the complex shape of stellarator coil, asymmetrical distributions were confirmed compared to the typical solenoid magnet. Total simulation times

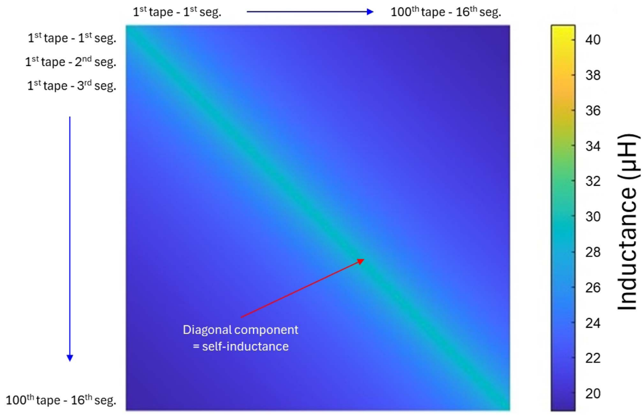

Fig. 3. Inductance matrix calculation results. Diagonal components represent the self-inductance of each element while other components are the mutual inductances.

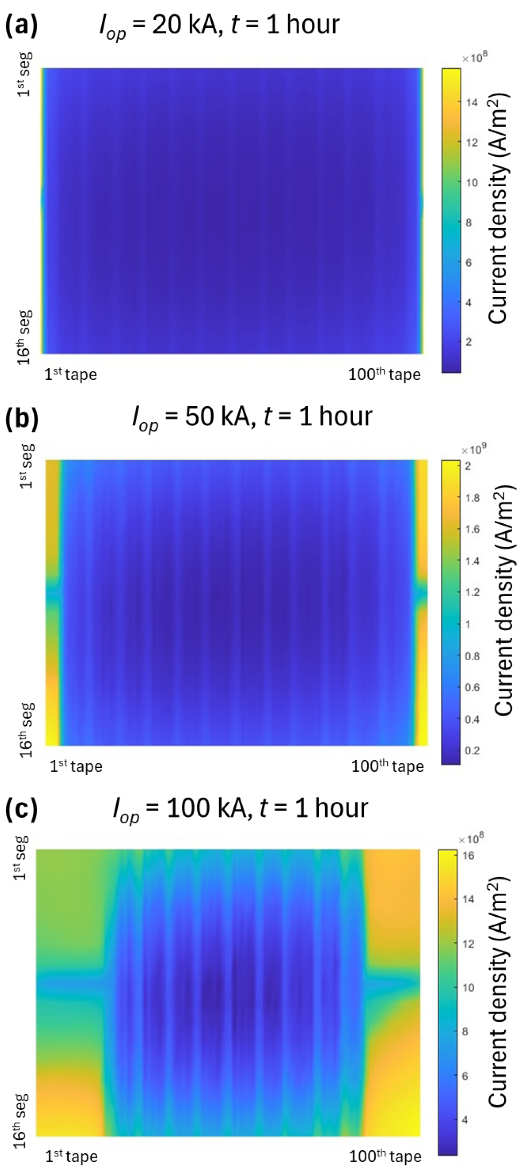

Fig. 4. Calculation results of current distribution on the cross-section of the coil at right after the charging for (a) 20 kA, (b) 50 kA, and (c) 100 kA cases.

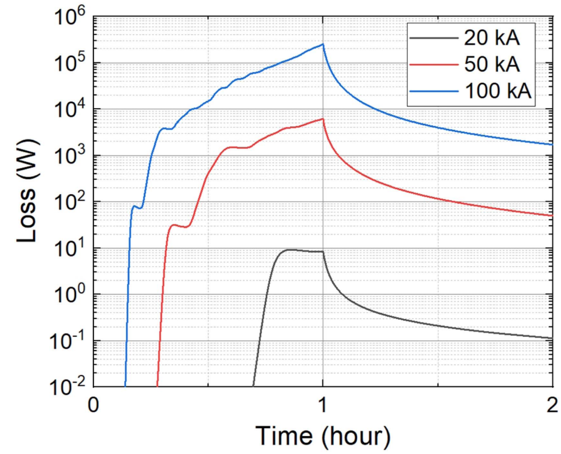

Fig. 5. AC loss calculation results for each simulation case. Peak loss was about 10 W for the lowest operating current while the values were significantly larger for another cases.

for two hours of operation scenario were 22, 36, and 57 minutes for the cases.

Based on current distribution, AC loss can be calculated by following equation:

$$\dot{Q} = \iiint \vec{E} \cdot \vec{J}\, dV \tag{2}$$

where $\dot{Q}$, $\vec{E}$, and $\vec{J}$ represent the AC loss, electrical field determined by power-law, and the current density, respectively. As shown in Fig. 5, peak value of AC loss was about 10 W for 20 kA case while the values were considerably larger for another cases. For the actual stellarator magnet operation, AC loss should be determined based on the current distribution of each module coil and magnetic field distribution. Our simulation showed that the magnet properties caused by the screening current can be calculated within an hour which is considerably short period of time. The analysis results can serve as a reference to quantitatively determine how slow the charging speed must be to reduce AC loss to a negligible level.

IV. Experimental Validation: 50-Turn Nonplanar NI Coil With Simplified Stellarator Shape

Although it would be fascinating to verify the model by building a real-scale magnet, it is not efficient or practical due to large amount of cost and time required. Therefore, we fabricated 1/20-scale stellarator coil as shown in Fig. 6. The shape of the coil was simplified due to excessive strain during scale-down. We arbitrarily removed some strain peak points to control the maximum strain less than 0.4% . The test coil was wound with SuNAM's 4-mm width conductor. The number of coil turns was 50, and no-insulation technique was incorporated to validate the circuit model. The aluminum coil bobbin was fabricated by metal 3D printing technology. The clamps were used to maintain the coil shape. The test coil was charged in the 77 K of liquid nitrogen bath and the measured contact resistivity was 120 $\mu\Omega\text{cm}^2$. To observe screening current induced voltage, we

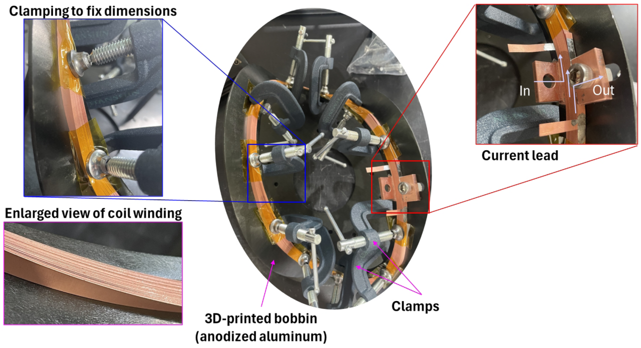

Fig. 6. Fabricated test coil with a simplified stellarator shape. A 50-turn single-pancake coil was wound with NI technique. To fix dimension of the coil, clamps were used as shown in the blue box. Red box indicates the current lead structure, and the pink box shows the winding results.

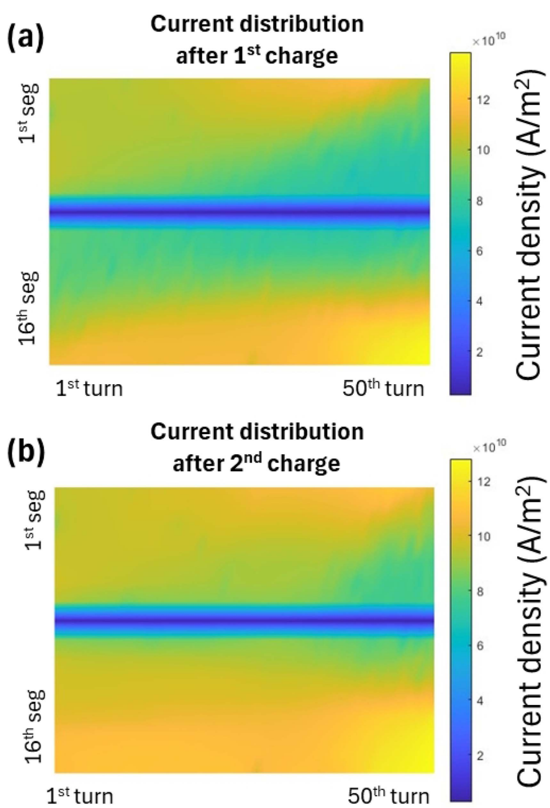

Fig. 7. Calculation results of current distribution on the cross-section of the test coil after (a) the first 50 A charge, and (b) the second one. The results show distinguishable differences.

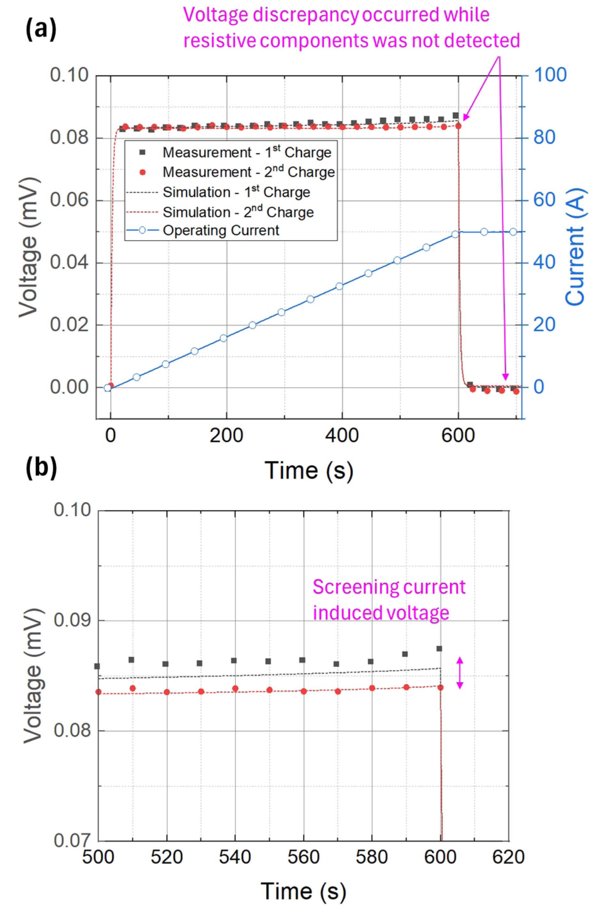

Fig. 8. Screening current induced voltage measurement results. Voltage profiles during the charging sequence showed the discernible discrepancy while voltage at current holding did not show any resistance.

repeatedly charged the coil without warming up. If we don‘t warm up the coil, then the residual screening current remains so we can observe different voltage profile between each charging process. The operating current of the coil was 50 A.

Using the same circuit model, we calculated current distribution as well as other parameters. The results clearly show the different current distribution for the first and second charging as shown in Fig. 7. This difference in current distribution caused the different voltage profiles. The voltage profiles of the first charge and the second charge showed distinguishable discrepancy as expressed in Fig. 8(a). However, when we held the current at 50 A, we cannot observe any resistive component inside the coil. We can clearly see the difference by this enlarged graph in Fig. 8(b). The circuit analysis results clearly reproduced the trend of the screening current induced voltage, verifying the accuracy of the circuit model and confirming its usefulness.

V. Conclusion

In this study, we developed and validated a numerical model for simulation of the screening current distribution in REBCO stellarator coils using a distributed-circuit model with widthwise segmentation of conductor. The number of circuit elements was reduced by applying the equipotential assumption along the conductor width, which can generally be applied. This model efficiently calculated the electromagnetic and thermal parameters such as current distribution and AC loss within a short period of calculation time. The experiment involving a 1/20-scale stellarator coil confirmed the accuracy of the model, especially in capturing the effects of screening current on voltage profiles during repeated coil operation. The results suggested that voltage measurement can be a useful tool for estimating screening current in high-temperature superconducting (HTS) magnets. Future work will focus on simulating the entire stellarator magnet system for more comprehensive analysis, as well as validating the effectiveness of simulation method by additional experiments.

REFERENCES

[1] T. Lécrevisse, X. Chaud, P. Fazilleau, C. Genot, and J.-B. Song, "Metal-as-insulation HTS coils," *Supercond. Sci. Technol.*, vol. 35, no. 7, 2022, Art. no. 074004.

[2] P.-H. Chen et al., "Watch-sized 12 tesla all-high-temperature-superconducting magnet," *J. Magn. Reson.*, vol. 357, 2023, Art. no. 107588.

[3] Y. Suetomi et al., "Quench and self-protecting behaviour of an intra-layer no-insulation (LNI) REBCO coil at 31.4 t," *Supercond. Sci. Technol.*, vol. 34, no. 6, 2021, Art. no. 064003.

[4] G. Kim et al., "Investigation on nonuniform current density and shape deformation affecting the magnetic field performance of a saddle-shaped no-insulation HTS cosine–theta dipole magnet," *Supercond. Sci. Technol.*, vol. 36, no. 8, 2023, Art. no. 084002.

[5] W. Lee, D. Park, J. Bascuñán, and Y. Iwasa, "Construction and test result of an all-REBCO conduction-cooled 23.5 T. magnet prototype towards a benchtop 1 GHz NMR spectroscopy," *Supercond. Sci. Technol.*, vol. 35, no. 10, 2022, Art. no. 105007.

[6] X. Zhang et al., "26.86-tesla direct-current magnetic field generated with an all-REBCO superconducting magnet," *Supercond. Sci. Technol.*, vol. 37, no. 8, 2024, Art. no. 085003.

[7] Y. Zhai, A. Otto, and M. Zarnstorff, "High current density cables for simpler HTS magnets in fusion energy systems," *IEEE Trans. Appl. Supercond.*, vol. 34, no. 5, Aug. 2024, Art. no. 4802407.

[8] A. Zappatore, G. De Marzi, and D. Uglietti, "Impact of hysteresis losses in hybrid (HTS-LTS) coils for fusion applications," *IEEE Access*, vol. 11, pp. 100465–100478, 2023.

[9] L. Muzzi et al., "Design and feasibility assessment of an HTS sector shaped high-current conductor for fusion coils," *IEEE Trans. Appl. Supercond.*, vol. 33, no. 5, 2023, Art. no. 4200106.

[10] N. Yanagi et al., "Feasibility of HTS magnet option for fusion reactors," *Plasma Fusion Res.*, vol. 9, pp. 1405013–1405013, 2014.

[11] H. Anand et al., "Modelling, design and simulation of plasma magnetic control for the spherical tokamak for energy production (STEP)," *Fusion Eng. Des.*, vol. 194, 2023, Art. no. 113724.

[12] Z. S. Hartwig et al., "The SPARC toroidal field model coil program," *IEEE Trans. Appl. Supercond.*, vol. 34, no. 2, Mar. 2024, Art. no. 0600316.

[13] R. F. Vieira et al., "Design, fabrication, and assembly of the SPARC toroidal field model coil," *IEEE Trans. Appl. Supercond.*, vol. 34, no. 2, Mar. 2024, Art. no. 0600615.

[14] N. Riva et al., "Development of the first non-planar REBCO stellarator coil using VIPER cable," *Supercond. Sci. Technol.*, vol. 36, no. 10, 2023, Art. no. 105001.

[15] D. Kingham and M. Gryaznevich, "The spherical tokamak path to fusion power: Opportunities and challenges for development via public–private partnerships," *Phys. Plasmas*, vol. 31, no. 4, 2024, Art. no. 042507.

[16] S. Hahn, D. K. Park, J. Bascuñán, and Y. Iwasa, "HTS pancake coils without turn-to-turn insulation," *IEEE Trans. Appl. Supercond.*, vol. 21, no. 3, pp. 1592–1595, Jun. 2011.

[17] S. Hahn et al., "45.5-tesla direct-current magnetic field generated with a high-temperature superconducting magnet," *Nature*, vol. 570, no. 7762, pp. 496–499, 2019.

[18] Y. Yanagisawa et al., "Effect of YBCO-coil shape on the screening current-induced magnetic field intensity," *IEEE Trans. Appl. Supercond.*, vol. 20, no. 3, pp. 744–747, Jun. 2010.

[19] M. C. Ahn, J. Jang, W. S. Lee, S. Hahn, and H. Lee, "Experimental study on hysteresis of screening-current-induced field in an HTS magnet for NMR applications," *IEEE Trans. Appl. Supercond.*, vol. 24, no. 3, Jun. 2014, Art. no. 4301605.

[20] Y. Yan, Y. Li, and T. Qu, "Screening current induced magnetic field and stress in ultra-high-field magnets using REBCO coated conductors," *Supercond. Sci. Technol.*, vol. 35, no. 1, 2021, Art. no. 014003.

[21] H. Ueda, H. Maeda, Y. Suetomi, and Y. Yanagisawa, "Experiment and numerical simulation of the combined effect of winding, cool-down, and screening current induced stresses in REBCO coils," *Supercond. Sci. Technol.*, vol. 35, no. 5, 2022, Art. no. 054001.

[22] D. Kolb-Bond et al., "Screening current rotation effects: SCIF and strain in REBCO magnets," *Supercond. Sci. Technol.*, vol. 34, no. 9, 2021, Art. no. 095004.

[23] S. Viarengo et al., "A new coupled electrodynamic T-A and thermal model for the critical current characterization of high-temperature superconducting tapes and cables," *IEEE Access*, vol. 11, pp. 107548–107561, 2023.

[24] K. Zhang, M. Ainslie, M. Calvi, R. Kinjo, and T. Schmidt, "Fully-staggered-array bulk Re-Ba-Cu-O short-period undulator: Large-scale 3D electromagnetic modelling and design optimization using AV and H-formulation methods," *Supercond. Sci. Technol.*, vol. 34, no. 9, 2021, Art. no. 094002.

[25] A. Arsenault, F. Sirois, and F. Grilli, "Efficient modeling of high-temperature superconductors surrounded by magnetic components using a reduced H–phi formulation," *IEEE Trans. Appl. Supercond.*, vol. 31, no. 4, Jun. 2021, Art. no. 6800609.

[26] V. M. Rodriguez-Zermeno et al., "Towards faster FEM simulation of thin film superconductors: A multiscale approach," *IEEE Trans. Appl. Supercond.*, vol. 21, no. 3, pp. 3273–3276, Jun. 2011.

[27] V. M. Zermeno, A. B. Abrahamsen, N. Mijatovic, B. B. Jensen, and M. P. Sørensen, "Calculation of alternating current losses in stacks and coils made of second generation high temperature superconducting tapes for large scale applications," *J. Appl. Phys.*, vol. 114, no. 17, 2013, Art. no. 173901.

[28] G. Kim et al., "Fast current distribution simulation method for no-insulation HTS coil with defects," *IEEE Trans. Appl. Supercond.*, vol. 32, no. 6, Sep. 2022, Art. no. 4602905.

[29] L. Qin et al., "Refined circuit model for current distribution of the no-insulation HTS insert magnet," *Supercond. Sci. Technol.*, vol. 34, no. 7, 2021, Art. no. 075002.

[30] T. Mato and S. Noguchi, "Effect comparison of different conductor widths in magnetic dam for protection of NI REBCO pancake coils," *IEEE Trans. Appl. Supercond.*, vol. 34, no. 3, May 2024, Art. no. 4701705.

[31] G. Kim et al., "A numerical method for spatially-distributed transient simulation to replicate nonlinear 'defect-irrelevant' behaviors of no-insulation HTS coil," *Supercond. Sci. Technol.*, vol. 34, no. 11, 2021, Art. no. 115004.

[32] G. Kim et al., "Distributed-circuit method for replication of fast-ramping of saddle-shaped REBCO dipole magnet wound with two-tape bundled conductor," *IEEE Trans. Appl. Supercond.*, vol. 34, no. 5, Aug. 2024, Art. no. 4000405.

[33] T. Wang et al., "Analyses of transient behaviors of no-insulation REBCO pancake coils during sudden discharging and overcurrent," *IEEE Trans. Appl. Supercond.*, vol. 25, no. 3, Jun. 2015, Art. no. 4603409.

[34] Y. Liu et al., "Study of contact resistivity of a no-insulation superconducting coil," *Supercond. Sci. Technol.*, vol. 34, no. 3, 2021, Art. no. 035009.

[35] F. W. Grover, "The calculation of the mutual inductance of circular filaments in any desired positions," *Proc. IRE*, vol. 32, no. 10, pp. 620–629, Oct. 1944.

[36] G. Kim et al., "Experimental study and frequency domain analysis on metal-insulation HTS coil," *IEEE Trans. Appl. Supercond.*, vol. 32, no. 4, Jun. 2022, Art. no. 4600505.

[37] G. Kim et al., "Analysis of nonuniform contact resistivity distribution on no-insulation HTS racetrack coil," *IEEE Trans. Appl. Supercond.*, vol. 33, no. 5, Aug. 2023, Art. no. 4601305.

[38] G. Kim et al., "Experimental study for modified lumped-circuit model to analyze saddle-shaped no-insulation HTS coil operated in overcurrent situation," *IEEE Trans. Appl. Supercond.*, vol. 34, no. 5, Art. no. 4600905, Aug. 2024.

[39] X. Wang et al., "Turn-to-turn contact characteristics for an equivalent circuit model of no-insulation ReBCO pancake coil," *Supercond. Sci. Technol.*, vol. 26, no. 3, 2013, Art. no. 035012.

[40] D. Hilton, A. Gavrilin, and U. Trociewitz, "Practical fit functions for transport critical current versus field magnitude and angle data from (RE) BCO coated conductors at fixed low temperatures and in high magnetic fields," *Supercond. Sci. Technol.*, vol. 28, no. 7, 2015, Art. no. 074002.